Comparison of Feedback Control Techniques for Torque-Vectoring Control of Fully Electric Vehicles

Leonardo De Novellis, *Member, IEEE*, Aldo Sorniotti, *Member, IEEE*, Patrick Gruber, and Andrew Pennycott

***Abstract*—Fully electric vehicles (FEVs) with individually controlled powertrains can significantly enhance vehicle response to steering-wheel inputs in both steady-state and transient conditions, thereby improving vehicle handling and, thus, active safety and the fun-to-drive element. This paper presents a comparison between different torque-vectoring control structures for the yaw moment control of FEVs. Two second-order sliding-mode controllers are evaluated against a feedforward controller combined with either a conventional or an adaptive proportional–integral–derivative (PID) controller. Furthermore, the potential performance and robustness benefits arising from the integration of a body sideslip controller with the yaw rate feedback control system are assessed. The results show that all the evaluated controllers are able to significantly change the understeer behavior with respect to the baseline vehicle. The PID-based controllers achieve very good vehicle performance in steady-state and transient conditions, whereas the controllers based on the sliding-mode approach demonstrate a high level of robustness against variations in the vehicle parameters. The integrated sideslip controller effectively maintains the sideslip angle within acceptable limits in the case of an erroneous estimation of the tire–road friction coefficient.**

***Index Terms*—Fully electric vehicle (FEV), sideslip angle, torque-vectoring (TV) control, yaw rate.**

I. Introduction

INDIVIDUALLY controlled powertrains in fully electric vehicles (FEVs) allow significant improvements not only in terms of vehicle architecture, packaging, and energy management but also from the viewpoint of vehicle dynamics design. The precise and highly responsive torque control of individual electric motor drives can have a major impact on the vehicle steady-state and transient handling response characteristics. Torque vectoring (TV) actuated through individual motor control is more effective than TV based on active differentials. In fact, TV differentials have limitations in terms of dynamic response, maximum allowable torque transfer, efficiency, and flexibility in the torque transfer direction in the case of a significant speed difference between the sun gears [1]. The design of the cornering response of FEVs can be carried out mainly at the control system level as the traditional tools for handling tuning (e.g. the adjustment of the suspension parameters) produce a marginal effect compared with the continuous TV actuation of the electric motor drives.

Full exploitation of the benefits of TV control for FEVs is only feasible with the implementation of more advanced controllers than those used in vehicle stability control systems today. Current systems are typically designed for friction brake actuation in emergency conditions without any particular requirement for smoothness of the intervention and, therefore, vehicle comfort or fun-to-drive [2]. However, stability controllers are evolving toward smooth continuous operation, particularly during significant braking and acceleration maneuvers. In this respect, in [3] alternative control structures for FEV TV control, with particular focus on linear parameter-varying gain-scheduled control, are discussed. The vehicle stability control systems installed in modern passenger cars are mainly based on feedback yaw rate controllers that intervene to recover a significant yaw rate deviation when a tolerance threshold between the reference value (mainly dependent on steering-wheel angle, vehicle velocity, and the estimated friction coefficient) and the measured value is exceeded. The usual method for evaluating the corrective yaw moment is a feedback controller for which the gains can be computed through various methodologies such as the Riccati equation [2]. In [4], a linear matrix inequality-based method for the design of a gain-scheduled yaw rate controller is presented. Other publications deal with advanced robust control techniques, such as generalized predictive control [5].

Furthermore, the controllers can regulate vehicle sideslip angle β, which can be estimated through an extended Kalman filter. The sideslip angle controllers are based on the theory of Shibahata (see the analyses in [6] and [7] for an overall idea), which demonstrates that the achievable vehicle yaw moment M_z, controlled by the driver through the steering-wheel angle, is a decreasing function of the magnitude of β. As a consequence, at high values of β, the driver no longer perceives a significant effect of the steering-wheel angle on the vehicle response. This can lead to driver reactions that can degrade vehicle stability.

The potential of electric motor drives in TV control can be exploited through the adoption of feedforward controllers that generate continuous reference yaw moments. The controllers must be coupled with feedback control structures that produce a yaw moment contribution starting from a continuous reference yaw rate, which, in turn, is based on precise tire–road

Manuscript received January 19, 2013; revised July 9, 2013 and December 10, 2013; accepted January 28, 2014. Date of publication February 10, 2014; date of current version October 14, 2014. This work was supported by the European Union's Seventh Framework Programme FP7/2007-2013 under Grant 284708. The review of this paper was coordinated by Prof. T. Shim.

The authors are with the University of Surrey, Surrey GU2 7XH, U.K. (e-mail: l.denovellis@surrey.ac.uk; a.sorniotti@surrey.ac.uk; p.gruber@surrey.ac.uk; a.pennycott@surrey.ac.uk).

Digital Object Identifier 10.1109/TVT.2014.2305475

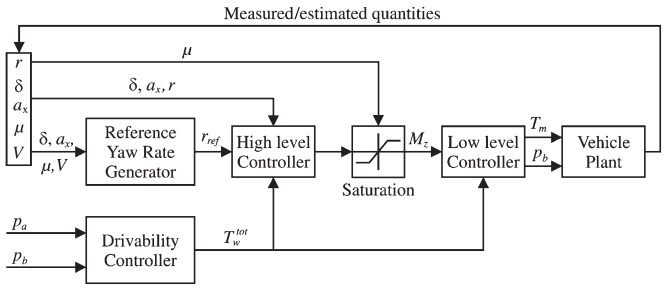

Fig. 1. Scheme of the proposed TV-controlled FEV.

friction coefficient estimation. Moreover, the feedback part of the controller, which is responsible for the generation of the reference yaw moment correction, must be smooth and robust against variations in the vehicle characteristics such as mass and yaw moment of inertia, and tire parameters and operating conditions, such as tire–road friction. Sliding-mode control is well-suited for this application since it can cope with systems characterized by significant uncertainty, and at the same time, its implementation does not require highly complex control laws. Although several publications have presented different formulations of sliding-mode controllers applied to vehicle yaw moment control (see [8] and [9]), a direct comparison of the performance of these control structures with conventional feedback controllers based on the proportional–integral–derivative (PID) algorithm is lacking.

In this paper, the structure of the yaw rate controller and its requirements for vehicle implementation are presented and described, together with a preliminary analysis of the yaw rate frequency response characteristics obtained from a single-track model under various linearization conditions. This aspect represents a point of novelty with respect to previous publications on the same subject [6], [10] and constitutes a useful tool for the TV control system designer. Furthermore, two different sliding-mode algorithms for yaw rate control are implemented and assessed against conventional PID and adaptive PID algorithms. The evaluation is carried out through an extensive analysis of maneuvers simulated by means of an experimentally validated vehicle model. Finally, the integration of yaw rate and sideslip angle controllers based on sliding mode into a single control structure is presented, and the effectiveness of this structure in limiting sideslip angle when the friction estimation required for yaw rate control fails is demonstrated by means of simulations.

II. Yaw Rate Control Structure

The structure of the yaw rate controller is shown in Fig. 1. The outputs of the controller are the wheel torques, which must be delivered by the electric motors and the friction brakes (when necessary) to achieve the reference yaw rate.

The controllers are designed for implementation on real vehicles developed within the European research project E-VECTOORC (*E*lectric *Ve*hicle *C*ontrol of Individual Wheel *T*orque for *O*n- and *O*ff-*R*oad *C*onditions) [11], [12]. Therefore, the design specifications and physical limits of the actuators and the energy storage unit have been carefully taken into account.

Yaw rate r, longitudinal acceleration a_x, accelerator pedal position p_a, brake pedal position p_b, and steering-wheel angle δ are commonly measured by on-board sensors and inertial platforms. Vehicle speed V and friction coefficient μ at the tire–road contact are estimated quantities. Since the estimation of vehicle speed, friction coefficient, and sideslip angle is not the subject of this paper, it is assumed that this estimation can be satisfactorily implemented (or unsatisfactorily, in the case of failure in tire–road friction estimation, as discussed in Sections IV and VI).

A. Design Requirements

In conditions of constant velocity, the adoption of a TV control system allows the achievement of a reference understeer characteristic significantly different to that of the baseline vehicle (i.e. the passive vehicle with constant torque split). For example, the understeer gradient at low to medium levels of lateral acceleration can be reduced to improve the fun-to-drive aspect, and the linear region of the vehicle response (representing an approximately constant understeer gradient) can be extended to enhance vehicle controllability in cornering conditions. Moreover, the maximum achievable lateral acceleration can be increased, as demonstrated by previous studies (see [13] and [14]). In any case, the controller has been designed to work according to different driving modes ("normal," "sport," and "economy"), selectable by the driver, each of them corresponding to a different set of understeer characteristics. The results of this paper refer to the "sport" driving mode.

In conditions of combined cornering and acceleration/deceleration, the TV system is required to compensate, as much as possible, the variation in vehicle response. This variation with traction/braking is caused by the longitudinal load transfer between the two axles and the interaction between lateral and longitudinal tire forces, according to the friction ellipse concept [15]. On conventional vehicles (without TV), the compensation of the variation in vehicle behavior is carried out by the driver through the steering-wheel angle. The parameters of the reference understeer characteristics, such as the understeer gradient and the maximum value of lateral acceleration, are selected according to the longitudinal acceleration of the vehicle [16], [17]. Finally, for consistent vehicle behavior in transient maneuvers, the variation in the frequency response characteristic of the system due to changing operating conditions has to be compensated by the controller.

To ensure the feasibility of the actual implementation of such a control system, the design has to cope with actuator saturation, which determines the maximum and minimum threshold values of the applicable yaw moment; these are variable and depend on the operating conditions, such as the tire–road friction coefficient (see the simplified scheme represented in Fig. 1), the maximum torque deliverable by the motors, and vehicle speed. The dependence on speed is indirect, as the maximum torque of the electric motors is a function of the motor speed beyond the base speed. Finally, the threshold limit value of the sideslip angle β_{TH}, which is evaluated, e.g. for safety reasons with the approaches presented in [17] and [18] or chosen according to the desired application (e.g. to achieve high levels of sustained and stable sideslip following the specification of the car maker), should not be exceeded.

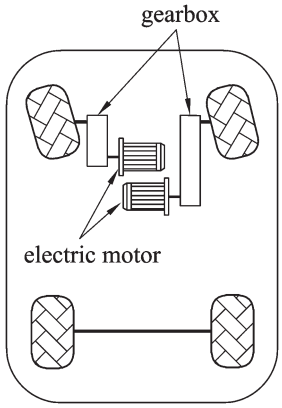

Fig. 2. Functional schematic of the case-study FWD electric vehicle.

TABLE I
MAIN ELECTRIC VEHICLE PARAMETERS

Symbol	Description	Quantity
M	Overall vehicle mass (including driver)	1963 kg
J_z	Vehicle yaw moment of inertia	2760 kgm^2
a	Front semi-wheelbase	1 m
b	Rear semi-wheelbase	1.6 m
c	Front and rear track width	1.625 m
h_{CG}	Height of the vehicle center of mass	0.66 m
$P_{M,MAX}$	Maximum electric motor power	114 kW
$n_{M,MAX}$	Maximum electric motor speed	14000 RPM
τ	Transmission gear ratio	10:1

TABLE II
TIRE PARAMETERS FOR HIGH-FRICTION CONDITIONS

Symbol	DESCRIPTION	Quantity
-	Tire A	235/55 R19
-	Tire B	255/35 R20
C_F	Cornering stiffness at $F_{z,NOM}$ (Tire A)	80844 N/rad
C_F	Cornering stiffness at $F_{z,NOM}$ (Tire B)	94813 N/rad
$F_{z,NOM}$	Nominal vertical force	5000 N
$F_{y,MAX}$	Maximum lateral force at $F_{z,NOM}$ (Tire A)	5254 N
F_{yMAX}	Maximum lateral force $F_{z,NOM}$ (Tire B)	5375 N

B. Plant and the Simulation Models

The case-study vehicle is a high-performance front-wheel-drive (FWD) sport utility vehicle. The drivetrain layout, shown in Fig. 2, consists of one on-board switched reluctance electric motor per wheel. The powertrains are connected to the wheels through single-speed transmissions and half-shafts with constant velocity joints.

The main vehicle characteristics are reported in Table I. Moreover, two different commercially available tires have been considered to assess the robustness of the yaw moment controller: Tire A is comfort oriented and Tire B is sports oriented. Specific tire parameters are provided in Table II.

To evaluate the vehicle dynamics behavior, a simulation model in the time domain was created through integration of the IPG CarMaker chassis module into the Simulink environment adopted for the development of the drivetrain model. The electric drivetrain dynamics have been considered by taking into account the stiffness of the half-shafts and the backlash in the transmission elements [19]. The electric motor drive has been modeled by including its torque slew rate, the air gap torque (calculated through a transfer function), and the windage losses (experimentally measured maps). The efficiency maps of the motor drives have been provided by the manufacturer. The vehicle dynamics model has been validated against extensive experimental tests in steady-state and transient conditions carried out at the proving ground in Lommel, Belgium [17].

For the design of the feedforward contribution of the controller, a simpler vehicle model has been considered based on a quasi-static formulation [17]. This consists of a set of algebraic equations based on kinematic and equilibrium relationships. The model considers eight degrees of freedom corresponding to the translational motions in the longitudinal and lateral directions, yaw and roll motions, and the four rotational motions of the wheels and the front drivetrains. By assuming that the time derivatives of the main state variables (e.g. vehicle sideslip, longitudinal slip ratio, and roll angle) are zero, the quasi-static model allows the computationally demanding forward time integration of the equations of motion to be omitted. This is particularly beneficial when static maps of the main physical quantities are needed for the automated derivation of the lookup tables for the feedforward controller. The quasi-static model has been validated against simulations with the CarMaker model and experimental data [14], [17].

C. Preliminary Analysis of the Vehicle Dynamics

The yaw rate transfer function of the vehicle without TV control (the so-called "baseline vehicle") can be obtained from the equations describing the lateral force and yaw dynamics of the single-track vehicle model [20]. Thus

$$\begin{cases} J_z\dot{r} = N_\beta\beta + N_r r + N_\delta\delta_w \\ mV(r+\dot{\beta}) = Y_\beta\beta + Y_r r + Y_\delta\delta_w. \end{cases} \tag{1}$$

In this equation, δ_w is the mean steer angle of the front wheels. The stability derivatives can be expressed as a function of the front and rear cornering stiffnesses, i.e. C_F and C_R, respectively, as

$$Y_\beta = C_{\mathrm{F}} + C_R; \qquad Y_r = \frac{aC_F - b\,C_R}{V}; \quad Y_\sigma = -C_F$$

$$N_\beta = a\,C_F - b\,C_R; \quad N_r = \frac{a^2C_F + b^2C_R}{V}; \quad N_\delta = -aC_F.$$

By rearranging the equations, the transfer function of the yaw rate dynamics becomes

$$\left.\frac{r}{\delta_w}(s)\right|_{\text{baseline}} = \frac{Ds+E}{As^2+Bs+C} \tag{2}$$

where coefficients $A-E$ are functions of the axle cornering stiffness (defined as the incremental ratio of the lateral force to the mean slip angle of the wheels on the same axle), the yaw moment of inertia, the vehicle mass, and the semi-wheelbases. Thus

$$A = mVJ_z; \quad B = -(mVN_r + Y_\beta J_z)$$

$$C = mVN_\beta + N_rY_\beta - N_\beta Y_r; \quad D = mVN_\delta$$

$$E = N_\beta Y_\delta - N_\delta Y_\beta.$$

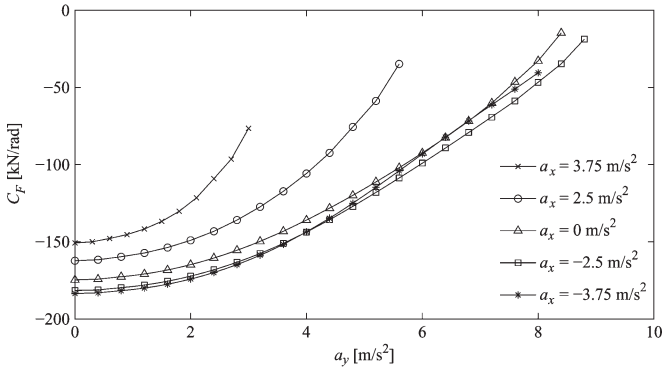

Fig. 3. Cornering stiffness of the front axle evaluated with the quasi-static model as a function of lateral acceleration for different values of longitudinal acceleration. Tire A has been used. The different trend of C_F for positive and negative values of a_x is due to the effect of the longitudinal load transfer in traction and braking conditions.

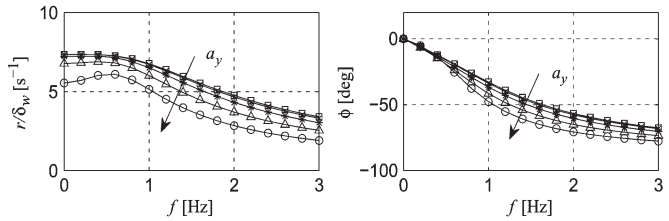

Fig. 4. Yaw rate frequency response evaluated for the baseline vehicle at different values of lateral acceleration, from $a_y = 0$ m/s^2 to $a_y = 6$ m/s^2, in steps of 1.5 m/s^2. The arrows point in the direction of increasing a_y values. Tire A has been used.

The variation of the vehicle frequency response as a function of the operating conditions in terms of longitudinal and lateral accelerations is discussed further below (see Figs. 4 and 5). This is achieved through variation of the terms C_F and C_R defining the coefficients of (2). In particular, by employing the quasi-static model described in Section II-B, it is possible to evaluate the cornering forces at the front and rear axles for the FWD case-study vehicle in different operating conditions. Therefore, at discrete points, the front- and rear-axle cornering forces have been locally linearized to evaluate the cornering stiffness of the baseline vehicle for the front and rear axles as a function of the longitudinal and lateral accelerations in trimmed conditions, as shown in Fig. 3. The cornering stiffness of the front axle is not subjected to a significant variation in braking conditions, as the reduction induced by the braking force is compensated for by the increase due to the load transfer from the rear to the front axle.

The effect of lateral acceleration a_y on the yaw rate dynamics (i.e. the yaw rate gain) is shown in Fig. 4. The steady-state gain decreases from 7.3 to 5.5 s^{-1}, and the damping ratio of the system varies from 0.9 to 0.8. At constant velocity, phase angle ϕ decreases with lateral acceleration, particularly for frequency values larger than approximately 0.5 Hz. Vehicle understeer increases with longitudinal acceleration a_x, since the steady-state gain decreases from 10.6 to 4.5 s^{-1}; at frequencies larger than about 1.2 Hz, the yaw rate transfer functions tend to overlap (see Fig. 5). Furthermore, for low values of frequency, the delay between the wheel steer angle and the yaw rate decreases with increasing a_x since the phase angle tends toward larger values.

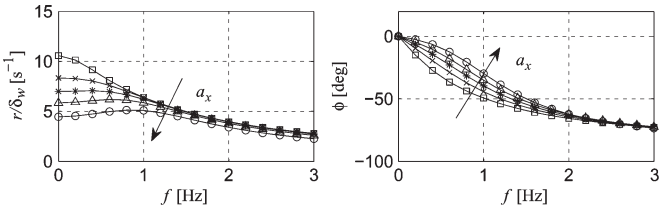

Fig. 5. Yaw rate frequency response evaluated for the baseline vehicle at $a_y = 4$ m/s^2 and different values of longitudinal acceleration, from $a_x = -2.5$ m/s^2 to $a_x = 2.5$ m/s^2, in steps of 1.25 m/s^2. The arrows point in the direction of increasing a_x values. Tire A has been used.

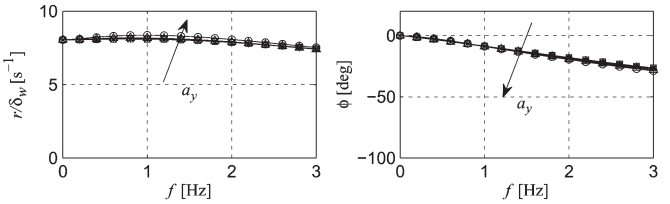

Fig. 6. Yaw rate frequency response evaluated for the controlled vehicle with constant-gain PID and feedforward contributions at different values of lateral acceleration, from $a_y = 0$ m/s^2 to $a_y = 6$ m/s^2, in steps of 1.5 m/s^2. The arrows point in the direction of increasing a_y values. Tire A has been used.

In the case of the controlled vehicle subject to a control yaw moment M_z, the yaw rate in the Laplace domain (s denoting the Laplace variable) can be expressed as

$$\begin{aligned} r(s) &= \left.\frac{r}{\delta_w}(s)\right|_{\text{baseline}} \delta_w + \frac{r}{M_z}(s) M_z(s) \\ &= \frac{(Ds+E)\delta_w}{As^2+Bs+C} + \frac{(F_2 s + F_1) M_z(s)}{As^2+Bs+C} \end{aligned} \tag{3}$$

with $F_2 = mV$ and $F_1 = -Y_\beta$. For example, M_z can include a feedforward contribution $M_{z,ff}(s)$ and the contribution $M_{z,PID}(s)$ of a PID controller. In this research, the feedforward contribution is the main element responsible for achieving the reference steady-state gain in conjunction with the PID controllers. Therefore, in this linearized example, $M_{z,ff}$ can be obtained starting from the equations of the linearized system. Thus

$$M_{z,ff} = \left(\frac{C r_{ref}}{\delta_w} - E\right)\frac{\delta_w}{F_1}. \tag{4}$$

The contribution of the feedback controller is $M_{z,PID}(s) = k_{PID}(s)(r(s) - r_{ref}(s))$, where r_{ref} is the reference yaw rate. r_{ref} can be a constant $r_{ref,s}$ in the frequency domain, for example, given by $r_{ref,s} = \delta_w/(VK^w_{U,ref} + L/V)$, where $K^w_{U,ref} = (\partial\delta_w/\partial a_y)_{ref}$ is the reference value of the understeer gradient at the wheel. Alternatively, the reference yaw rate can be expressed as a first-order transfer function [18] such as $r_{ref}(s) = r_{ref,s}/(1+\tau s)$, where τ is the time constant of the first-order yaw rate reference. The transfer function of the yaw rate gain for the controlled vehicle including feedforward and PID is then

$$\frac{r}{\delta_w} = \frac{f_z(s)\left[\frac{M_{z,ff}}{\delta_w}(s) + \frac{r_{ref}}{\delta_w}(s) k_{PID}(s)\right] + \left.\frac{r}{\delta_w}(s)\right|_{\text{baseline}}}{1 + f_z(s) k_{PID}(s)} \tag{5}$$

with $f_z(s) = (r/M_z)(s)$.

Figs. 6 and 7 show the frequency response of the overall system evaluated through (5) at different values of a_x and a_y.

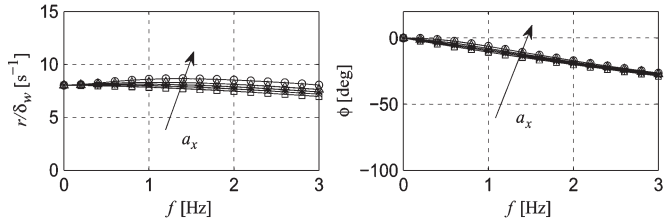

Fig. 7. Yaw rate frequency response evaluated for the controlled vehicle with constant-gain PID and feedforward contributions at different values of longitudinal acceleration, from $a_x = -3.75$ m/s^2 to $a_y = 3.75$ m/s^2, in steps of 1.25 m/s^2. The arrows point in the direction of increasing a_x values. Tire A has been used.

The reference yaw rate has been obtained at $V = 90$ km/h considering the value of $K^w_{U,ref} = 0.04$ degs^2/m constant with a_x and a_y. The following gains have been adopted: $k_P = 80$ kNms/rad, $k_I = 0.004$ Nm/rad, and $k_D = 0.8$ Nms^2/rad. The variation in the yaw rate transfer function is strongly attenuated, except at extreme values of longitudinal and lateral accelerations, compared with the results shown in Figs. 4 and 5. Moreover, the controlled system is characterized by a general reduction in the magnitude of the phase angles. Additionally, as the variation of the vehicle cornering response is very well compensated (see Figs. 6 and 7), a gain scheduling approach as a function of a_x and a_y is expected to produce only a small improvement relative to a constant gain PID controller (with respect to a_x and a_y), which will be adopted in the rest of this paper. Some gain scheduling of the PID gains is required as a function of vehicle speed in any case (when considering maneuvers with a significant speed range), but this is already well known [10] and not relevant to this paper, which focuses on maneuvers from an initial vehicle speed of 90 km/h and covering a relatively limited speed range. These preliminary conclusions will be verified in the following sections, in which the limitations of the actuated M_z (which can significantly change the results) and the anti-windup conditions on the controller are introduced.

D. Reference Yaw Rate

This section describes the methodology for the definition of $r_{ref,S}$ for the controller implemented on the real vehicle with nonlinear dynamics. A target understeer characteristic is defined in terms of an analytical function relating the dynamic steering-wheel angle $\delta_{dyn} = \delta - \delta_{kin}$ (where δ is the actual steering-wheel angle, and δ_{kin} is the kinematic steering-wheel angle) to the lateral acceleration a_y. Therefore, (6) is proposed, which is based on the following three characteristic parameters: the understeer gradient $K_U = \partial\delta_{dyn}/\partial a_y$; the threshold value a^*_y, which defines the upper limit of the linear part of the understeer characteristic; and the maximum lateral acceleration achievable in trimmed conditions $a_{y,MAX}$. Thus

$$a_y = \begin{cases} \frac{1}{K_U}\delta_{dyn}, & \text{if } \delta_{dyn} < a^*_y K_U \\ a_{y,MAX} + \left(a^*_y - a_{y,MAX}\right) & \\ \quad \times e^{\frac{K_U a^*_y - \delta_{dyn}}{\left(a_{y,MAX} - a^*_y\right)K_U}}, & \text{if } \delta_{dyn} \geq a^*_y K_U \end{cases} \tag{6}$$

where $a_{y,MAX} = a_{y,MAX}(\mu, a_x)$, and $a^*_y = a^*_y(\mu, a_x)$. The terms K_U, a^*_y, and $a_{y,MAX}$ can be chosen according to the control design requirements, as previously mentioned in Section II-A, as functions of a_x and μ. In particular, the same value of K_U at different values of the longitudinal acceleration has been considered, to achieve the compensation of the variation of the understeer gradient in traction and braking conditions. Using (6), the steady-state value of the reference yaw rate is given by

$$r_{ref,S} = \frac{a_y}{V}. \tag{7}$$

Equations (6) and (7) allow the generation of a lookup table for the reference yaw rate as a function of vehicle speed V, steering-wheel angle, longitudinal acceleration, and friction coefficient at the tire–road contact. To prevent excessive control action for high-frequency steering-wheel inputs, the output of the lookup table is multiplied by a first-order factor with $\tau = 0.3$ s.

E. Control Strategies

Four different approaches for the design of the yaw moment controller generating M_Z are considered and evaluated as follows:

- PID control with feedforward contribution;
- adaptive PID control with feedforward contribution [22];
- second-order sliding-mode (SOSM) control based on the suboptimal algorithm (without feedforward contribution) [23]–[25];
- SOSM control based on the twisting algorithm (without feedforward contribution) [26], [27].

To limit the analysis to the objective comparison of the four yaw moment control strategies, this paper is focused on maneuvers that do not require friction brake intervention (i.e. traction conditions), such that the assessment of the controllers is independent from the wheel torque distribution algorithm and the brake-blending algorithm. As a consequence, the drivetrain torques at the front wheels, i.e. T_{LF} and T_{RF}, are expressed as

$$\begin{aligned} T_{LF} &= T_m - \frac{M_z R}{c} \\ T_{RF} &= T_m + \frac{M_z R}{c} \end{aligned} \tag{8}$$

where R is the laden radius of the tire, and T_m is the mean wheel torque necessary for vehicle propulsion. T_m is evaluated by the vehicle drivability controller starting from the accelerator pedal position p_a defined by the driver model (see Fig. 1). The end goal of this paper is to see whether there is any real benefit that can be derived from the additional robustness of adaptive PID or sliding-mode formulations (recently adopted by several academic authors) against a simple PID with constant gains, for maneuvers in a well-defined speed range.

III. Design of the Yaw Rate Controllers

A. PID Controller

The feedforward contribution working together with the PID controller is based on lookup tables in terms of δ, a_x, and μ. The tables were obtained with the quasi-static vehicle model [14] using an optimization routine to derive the control yaw

moment that yields the desired set of understeer curves [17]. In traction conditions, the reference characteristics have a reduced understeer gradient, a wider linear region, and a larger maximum value of lateral acceleration with respect to the baseline vehicle.

The constant gains of the conventional PID have been tuned starting from the frequency response characteristic of the open-loop system through specifications in terms of the phase and gain margins, and the requirements of the closed-loop tracking bandwidth. An anti-windup system has been included for the management of the control action saturation [28].

B. Adaptive PID Controller

The adaptive PID control proposed in [22] is used here for the vehicle yaw moment control. The particular control formulation derives from the theory of adaptive interaction and an approximation of the Frechet tuning algorithm. The gains of the three-term controller (k_P, k_D, and k_I) are updated as a function of the yaw rate error:

$$\begin{aligned} \dot{k}_P &= -\gamma_P e^2 \\ \dot{k}_I &= -\gamma_I e \int e\, dt \\ \dot{k}_D &= -\gamma_D e\dot{e}. \end{aligned} \tag{9}$$

The initial values for the gains are calculated according to the conventional guidelines and principles for system stability and tracking bandwidth outlined in the previous section. The relevant adaptation coefficients were determined through a sensitivity analysis. The conditions for the Lyapunov stability of this control structure are presented in [22]. The system must have a structure of the form $ay^{(n)} = u$, with the following conditions: 1) $a > 0$; 2) dominant order $n \leq 2$; 3) availability of signals y and $y^{(1)}$; and 4) the reference trajectory and its first n derivatives are bounded and piecewise continuous. These properties are satisfied for the specific application as $J_z > 0$ and known (with some uncertainty depending on the payload), and the overall yaw moment due to vehicle longitudinal and lateral forces can be considered as the input u to the system. In the specific project, the stability of the adaptation scheme has been empirically verified during the tuning process.

C. Suboptimal SOSM

The main advantage of SOSM control is the ability to achieve the robustness typical of conventional sliding-mode control while avoiding control input chattering, which can compromise vehicle comfort and drivability. Considering a double integrator system including state variables $y_1(t)$ and $y_2(t)$

$$\begin{aligned} \dot{y}_1(t) &= y_2(t) \\ \dot{y}_2(t) &= \Phi(\cdot) + \Gamma(x,t)v(t) \end{aligned} \tag{10}$$

in a neighborhood of the sliding manifold $S(x,t) = y_1(t) = 0$, the uncertain terms Φ and Γ are bounded by known positive constants, i.e.

$$\begin{aligned} |\Phi(\cdot)| &\leq \tilde{\Phi} \\ 0 < \tilde{\Gamma}_1 &\leq \Gamma(x,t) \leq \tilde{\Gamma}_2. \end{aligned} \tag{11}$$

Depending on the relative degree between the sliding variable $S(x,t)$ and the control input $u(t)$, $v(t)$ may represent either the actual control action or its time derivative [29]; in the former case (relative degree 2), the control law will be discontinuous, whereas the latter case (relative degree 1), which is also referred to as the antichattering case, leads to a continuous control action [23], [24]. Hence, for the purpose of vehicle yaw moment control, system (10) is described as a relative degree-1 formulation, so that chattering, which is the main issue of sliding-mode control applications, is prevented. In fact, the discontinuity is transferred to the time derivative of the yaw moment and is absent on the yaw moment itself, calculated by integration in the time domain. This is ideal for the application as it allows conjugating robustness without chattering. The single-track model (see [8] and [30] is recalled to define the sliding surface as $S_r = r - r_{ref}$. Thus

$$\begin{aligned} \dot{y}_1 &= \dot{S}_r(t) = \frac{(aF_{yF}(t) - bF_{yR}(t) + M_z(t))}{J_z} - \dot{r}_{ref}(t) \\ \dot{y}_2 &= \ddot{S}_r(t) = \Phi + \Gamma v(t) \end{aligned} \tag{12}$$

with $\Gamma = 1$, $v(t) = \dot{M}_z(t)/J_z$, and $\Phi = (a\dot{F}_{yF}(t) - b\dot{F}_{yR}(t))/J_z - \ddot{r}_{ref}(t)$. According to the suboptimal sliding-mode algorithm, the control law assumes the form

$$\dot{M}_z(t) = -J_z k_r \text{sign}\left[S_r(t) - 0.5 S_r(t_{Mk})\right] \tag{13}$$

where t_{Mk} is defined as the time corresponding to the last singular value of $S_r(t)$, i.e. $\dot{S}_r(t_{Mk}) = 0$, with the constraint $k_r > 2\widetilde{\Phi}$.

After algebraic manipulation and using a simple expression for the reference yaw rate, Φ becomes

$$\Phi = \left[\dot{\beta}(aC_F - bC_R) - \dot{\delta}_w a C_F\right]/J_z - \ddot{\delta}_w/(VK_U^w + L/V). \tag{14}$$

In (14), the time derivatives of the wheel steer angle δ_w depend on the variation of the actual steering-wheel input. These terms can be very large compared with the other terms of (14). This has been verified through vehicle dynamics simulations, including the computation of (14) during typical transient maneuvers. In particularly critical situations, such as the step steer, the terms in (14) assume very significant values during the application of the steering-wheel input. However, they tend to rapidly decrease following the main input application event. As a result, a neighborhood of the sliding surface $S_r = 0$ can be found, in which the condition $k_r > 2\widetilde{\Phi}$ is satisfied for relatively small values of k_r. Such a sliding mode has only a local attraction property in the sense that the sliding motion of the system on the surface occurs after a certain time delay. On the other hand, the limits of the achievable control yaw moment due to actuator saturation demand a careful choice of the control gain, i.e. k_r, to prevent bang-bang control actuation due to the frequent actuator saturation. The saturation of M_z is considered by implementing the desaturation strategy presented in [32]

$$M_z\left(t_s^+\right) = \begin{cases} M_{z,MAX}, & M_z\left(t_s^-\right) > M_{z,MAX} \\ M_{z,MIN}, & M_z\left(t_s^-\right) < M_{z,MIN} \\ M_z\left(t_s^-\right), & M_{z,MAX} \geq M_z\left(t_s^-\right) \geq M_{z,MIN} \end{cases} \tag{15}$$

with t_s being the switching time, namely, $S_r(t_s)=0.5S_r(t_{Mk})$. In the actual implementation of the controller, a value $k_r = 20$ rad/s^3 is chosen. In the practical implementation, some residual oscillations in the sliding-mode controller can occur, particularly if the sampling time of the yaw rate signal is quite high (e.g. 10 ms) or different from that of the reference yaw rate. This phenomenon is similar to the so-called "ringing effect" that is typical of the digital implementation of sliding-mode control. A steep saturation function has been adopted for approximating the sign function in (13) and to damp out the residual oscillations [30].

D. Twisting SOSM

A description of the twisting algorithm used in this research is presented in [26] and [27]. The implementation follows the same approach as the suboptimal sliding mode, with the control law given by the relationship

$$\dot{M}_z = \begin{cases} -k_m J_z \text{sign}\left(S_r(t)\right), & S_r\dot{S}_r(t) \le 0 \\ -k_M J_z \text{sign}\left(S_r(t)\right), & S_r(t)\dot{S}_r(t) > 0 \end{cases} \tag{16}$$

with the following constraints: $k_M > k_m$; $k_m > (4\widetilde{\Gamma}_2 M_{z,MAX}^2)/(J_z^2 S_r(0))$; $k_m > (\widetilde{\Phi}/\widetilde{\Gamma}_1)$; $\widetilde{\Gamma}_1 k_M - \widetilde{\Phi} > \widetilde{\Gamma}_2 k_m + \widetilde{\Phi}$.

Desaturation strategy (15) satisfies condition $|M_z| \le M_{z,MAX}$ for the application of the twisting algorithm in the form (16). Moreover, as $\widetilde{\Gamma}_1 = \widetilde{\Gamma}_2 = 1$, the same conclusions on the magnitude of $\widetilde{\Phi}$ as in Section III-C can be drawn. The values of $k_m = 10$ rad/s^3 and $k_M = 32$ rad/s^3 have been selected.

IV. Integrated Yaw Rate and Sideslip Angle Controller

In general, the value of the sideslip angle can be kept within the stability limits of the vehicle through a yaw rate controller if the friction coefficient at the tire–road contact is accurately estimated and a correct reference yaw rate is generated. Under these conditions, yaw rate feedback control is sufficient to ensure safe handling and driving behavior. However, if the friction estimation is erroneous or the calculated reference yaw rate is excessive for the actual operating conditions, the vehicle behavior may become unstable. In such cases, safety can be ensured if a countermeasure is activated, which prevents the vehicle sideslip angle from exceeding the stability threshold.

As previously mentioned, sideslip angle estimation is not the subject of this paper; therefore, it is assumed that this estimation can be satisfactorily implemented, even if this is actually a challenging task. Some recent publications [35] show potential improvement in sideslip angle estimation achievable through the integration of the information from the Global Positioning System and the on-board sensors commonly installed in vehicles equipped with vehicle dynamics control systems.

A novel control algorithm is developed, which combines yaw rate control through the suboptimal SOSM approach with sideslip angle control. In contrast to previous research [9], the central idea here is to have a yaw moment controller based on yaw rate regulation and a sideslip angle controller that only operates when a certain threshold value of the sideslip angle β_{TH} is exceeded, without decelerating the vehicle.

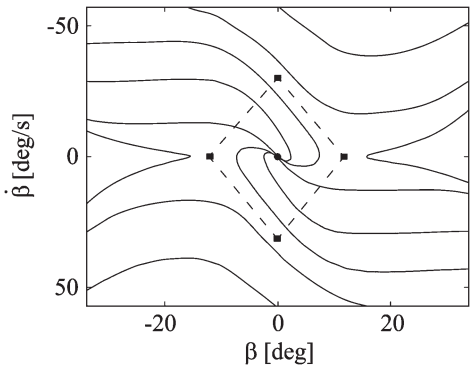

Fig. 8. Qualitative trend of the phase plane trajectories. The stability region is indicated with dashed lines.

The sideslip angle controller, which is implemented as a sliding-mode algorithm, aims at a sliding motion on the surface $S_\beta = 0$, with

$$\begin{aligned} S_\beta &= \beta - \beta_{TH} \\ \dot{S}_\beta &= \frac{F_{yF}(t) + F_{yR}(t)}{mV} - r - \dot{\beta}_{TH} \\ \ddot{S}_\beta &= \Phi_\beta + \Gamma_\beta v_\beta(t) \end{aligned} \tag{17}$$

where $\Phi_\beta = ((\dot{F}_{yF}(t) + \dot{F}_{yR}(t))/mV) - \ddot{\beta}_{\text{TH}} - ((aF_{yF}(t) - bF_{yR}(t))/J_z)$, $\Gamma_\beta = 1$, and $v_\beta(t) = -M_{z,\beta}(t)/J_z$. In this case, the relative degree between the sliding surface S_β and the control action $M_{z,\beta}$ is 2, and therefore, a resulting discontinuous control law is expected. According to the suboptimal sliding-mode algorithm, the control law is expressed as

$$M_{z,\beta}(t) = J_z k_\beta \text{sign}\left[S_\beta(t) - 0.5S_\beta(t_{Mk,\beta})\right]. \tag{18}$$

The choice of β_{TH} and $\dot{\beta}_{TH}$ can be determined by evaluating the stability regions in the phase plane $\beta - \dot{\beta}$ for the bicycle model (see Fig. 8) and considering a reasonable safety factor. The stability region is then approximated as a rhomboid [18]. To find the boundary of the uncertain term Φ_β in (17), the same method adopted in Section III-C for the time derivative of the cornering forces is applied. The term $\ddot{\beta}_{TH}$ of Φ_β, due to the linear relationship between β_{TH} and $\dot{\beta}_{TH}$, is limited, except when $\beta = 0$ or $\dot{\beta} = 0$, which are verified only for a very short amount of time in the actual implementation of the controller. In case of significant deviations from β_{TH}, the vehicle can be stabilized only by reducing the torque demand, i.e. slowing down the vehicle.

The final expression of the control yaw moment for the integrated yaw rate and sideslip angle controller has the form

$$M_z(t) = \rho_1 \left(M_{z,r}(t) - M_{z,\beta}(t)\right) + M_{z,\beta}(t) \tag{19}$$

with $M_{z,r}$ and $M_{z,\beta}$ given, respectively, by (13) and (18), while to ensure a smooth transition between the two different control actions, the term ρ_1 is expressed as

$$\ln \rho_1 = -\rho_2 e_\beta \tag{20}$$

$$e_\beta = \begin{cases} |S_\beta|, & |\beta| > |\beta_{TH}| \\ 0, & |\beta| \le |\beta_{TH}|. \end{cases} \tag{21}$$

In this analysis, $k_\beta = 5$ rad/s^2 and $\rho_2 = 100$ rad^{-1}, and the vertices of the rhomboid region have been chosen as $|\beta_{TH,MAX}| =$ 5 deg and $|\dot{\beta}_{TH,MAX}| = 24$ deg/s [36].

V. Assessment of the Performance of the Yaw Rate Controllers

The performance of the yaw rate control systems is assessed through indexes related to the control error $e(t) = r - r_{ref}$ and the control action $u(t) = M_z$. In particular, the following indexes are used during the relevant phases of the selected maneuvers:

- integral of the absolute value of the error: $IAE = \int_0^{t_m} |e(t)|dt$;
- integral of the time-weighted absolute value of the error: $ITAE = \int_0^{t_m} t|e(t)|dt$;
- integral of the absolute value of the control action: $IACA = \int_0^{t_m} |u(t)|dt$.

The $ITAE$ criterion complements the IAE criterion as, for example, the minimization of the IAE during a step steer can result in a response with a relatively small overshoot but a long settling time because the IAE weights all errors equally, independently of time [33].

To assess the performance of the different controllers in a simple and objective manner, a dimensionless performance-weighted function PWF has been defined as

$$PWF = \widetilde{w}_1 IAE + \widetilde{w}_2 ITAE + \widetilde{w}_3 IACA \qquad (22)$$

where $\widetilde{w}_1 = w_1/(r_{TH}t_m)$, $\widetilde{w}_2 = w_2/(r_{TH}t_m^2)$, and $\widetilde{w}_3 = w_3/(M_{z,MAX}t_m)$. $M_{z,MAX}$ is the maximum feasible absolute value of the control yaw moment. A reasonable threshold value of the yaw rate $r_{TH} = 0.02$ rad/s has been considered; t_m is the time duration of the relevant part of the considered maneuver. With such a formulation, $w_1 + w_2 + w_3 = 1$. The weights have been chosen to prioritize the achievement of the reference yaw rate with respect to the minimization of the control action.

Different tests have been simulated with the CarMaker vehicle model, in both steady-state and transient conditions. In the model, the yaw moment is generated by the different drivetrain torques on the front axle. Robustness is assessed by varying the vehicle weight and the friction coefficient at the tire–road contact and considering the two different tire typologies mentioned in Table II.

A. Ramp Steer Maneuver

The understeer characteristics of the investigated vehicles (i.e. baseline vehicle and the vehicle setups with the four different feedback controllers) are evaluated with ramp steer maneuvers (according to [34]) simulated with the Simulink-CarMaker model at a constant vehicle speed of $V = 90$ km/h. For the simulations, the target understeer gradient (at the steering wheel) is selected to be smaller than that of the baseline vehicle, i.e. $K_U = 12$ deg/g. Moreover, the linear section of the steering-wheel angle against the lateral-acceleration curve is selected to extend up to $a_y^* = 7.5$ m/s^2, and the asymptotic value of maximum lateral acceleration is increased to $a_{y,MAX} = 9.5$ m/s^2.

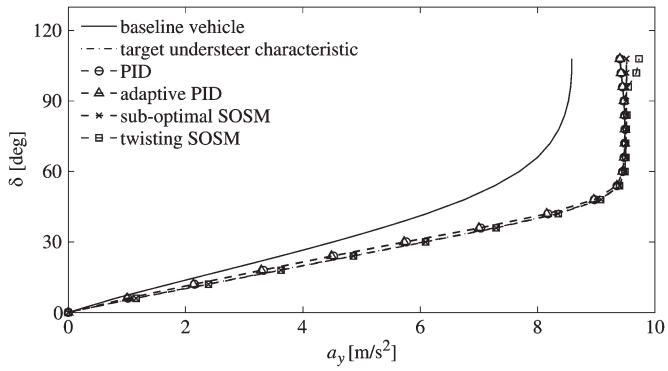

Fig. 9. Understeer characteristics evaluated at $V = 90$ km/h for (solid line) the baseline vehicle and for the controlled vehicle equipped with different yaw rate controllers in high-friction conditions. Tire A has been used.

TABLE III
PWF Values for Ramp Steer Tests

	$\mu = 1$ $m = 1963$ kg		$\mu = 0.5$ $m = 1963$ kg		$\mu = 1$ $m = 2363$ kg	
	Tire A	Tire B	Tire A	Tire B	Tire A	Tire B
PID	0.2	0.27	0.14	0.2	0.42	0.6
adaptive PID	0.2	0.27	0.15	0.2	0.44	0.6
sub-optimal SOSM	0.1	0.08	0.02	0.03	0.2	0.5
twisting SOSM	0.15	0.09	0.02	0.025	0.2	0.5

As indicated in Fig. 9, for the majority of the lateral-acceleration range, the sliding-mode algorithms perform better than the conventional PID and adaptive PID controllers in terms of tracking the reference cornering behavior. In particular, the suboptimal SOSM algorithm allows following the target understeer curve (see dotted-dashed line in Fig. 9) very closely. In addition, the overall tracking performance is satisfactory for the twisting SOSM algorithm, although a deviation from the reference characteristic is noticeable between $\delta = 90$ deg and $\delta = 110$ deg, which can lead to an undesired loss of vehicle stability.

Table III compares the performance of the different controllers and their robustness during ramp steer maneuvers. In the case of the PID and adaptive PID controllers, close matching is achieved due to the efficacy of the feedforward contribution, obtained from the simplified quasi-static model, which represents the overall vehicle with satisfactory accuracy. The PID controllers without the feedforward contribution would not be able to provide a good tracking performance of the reference understeer characteristic during the maneuver. The adaptive PID does not deliver any advantage when compared with the basic PID controller. The PID controller results for $\mu = 0.5$ were obtained by modifying the feedforward contribution as a function of the tire–road friction coefficient (see Section III-A). No adaptation of control parameters is required by the SOSM controllers (which do not require any feedforward contribution).

The suboptimal SOSM shows better performance also in the asymptotic region of the understeer characteristic, leading to a smaller error with respect to the reference yaw rate, as shown in Table III. The suboptimal SOSM is insensitive to the variation of the tire friction coefficient. However, the tracking performance is significantly influenced (PWF increases by

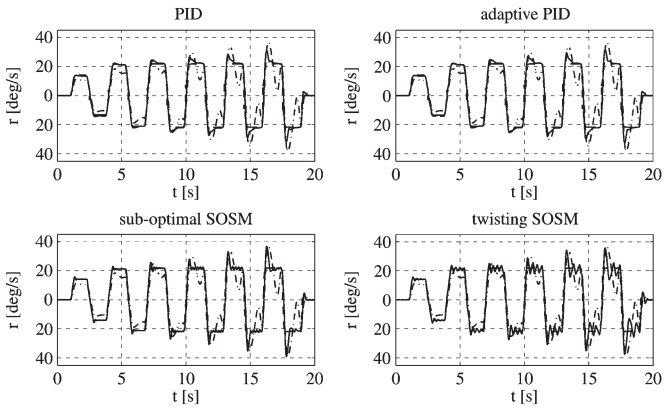

Fig. 10. Yaw rate r evaluated at $V = 90$ km/h during the sequence of step steer tests for different yaw rate controllers. (Solid line) Actual yaw rate. (Dashed line) Trend of the reference yaw rate. (Dotted-dashed line) Baseline vehicle behavior. Tire A has been used.

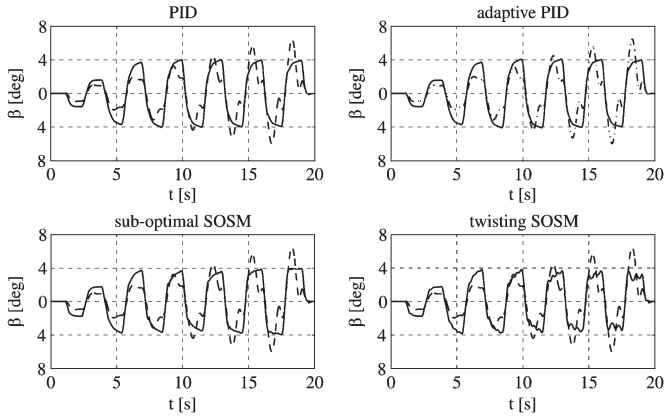

Fig. 11. Sideslip angle β evaluated at $V = 90$ km/h during the sequence of step steer tests for (solid line) different yaw rate controllers and (dashed line) the baseline vehicle. Tire A has been used.

TABLE IV
PWF VALUES FOR SEQUENCE OF STEP STEER TESTS

	$\mu = 1$ $m = 1963$ kg		$\mu = 0.5$ $m = 1963$ kg		$\mu = 1$ $m = 2363$ kg	
	Tire A	Tire B	Tire A	Tire B	Tire A	Tire B
PID	0.83	1.18	0.56	0.62	0.94	1.4
adaptive PID	0.88	1.19	0.56	0.62	0.94	1.4
sub-optimal SOSM	0.94	0.95	0.93	1.14	0.86	1.07
twisting SOSM	1.27	1.6	1.44	1.53	1.2	1.5

a factor of 6 for Tire B) by the variation of vehicle mass, which also affects the control performance when different tires are used. In any case, even when Tire B is considered with the increased vehicle mass, the tracking performance of the suboptimal SOSM remains marginally better than that achieved by the PID controllers. No significant effect of the tire type on the suboptimal controller performance can be observed for the nominal value of vehicle mass.

B. Sequence of Step Steer Maneuvers

The vehicle behavior in transient conditions over a wide range of yaw rate values, and up to the saturation point corresponding to the asymptote of the understeer characteristic, is evaluated with a sequence of fast-steering inputs of increasing amplitude. The values of the actual yaw rate and the reference yaw rate for each feedback controller are shown in Fig. 10. The trend in the yaw rate of the baseline vehicle is also overlapped and plotted as dotted-dashed lines.

Table IV presents the values of PWF for the sequence of step steer tests carried out with different tire–road friction coefficients (0.5 and 1), vehicle mass values (1963 and 2363 kg), and two tire types (A and B). As previously specified, the reference yaw rate and the feedforward contribution of the reference yaw moment were updated according to the different friction conditions. Under nominal operating conditions ($\mu = 1$, $m = 1963$ kg), the PID and adaptive PID show smaller values of PWF than the sliding-mode algorithms. Indeed, in the case of the sliding-mode controllers, large overshoots (suboptimal SOSM) and oscillations (twisting SOSM) occur at large steering-wheel angle steps, leading to an increase in the PWF parameter compared with the other controllers, giving rise to potential problems in terms of real vehicle drivability and safety. However, when the tire type is changed or when the vehicle mass is increased ($\mu = 1$, $m = 2363$ kg), the feedforward contribution (used in the case of the PID controllers but absent in the sliding-mode controllers) loses its effectiveness, whereas the suboptimal SOSM algorithm generally shows good adaptation capabilities. On average, PWF is marginally higher for the suboptimal SOSM than for PID; however, the variance of the PWF among the six test cases is lower for the suboptimal SOSM controller.

Fig. 11 shows that the value of the sideslip angle for the controlled vehicle is moderate and smaller than that of the baseline vehicle at large yaw rate values. In contrast, at smaller yaw rates, the controlled vehicle shows larger values of sideslip angle than the baseline vehicle since the relevant target understeer behavior is different (i.e. $K_{U,TV} < K_{U,\mathrm{baseline}}$).

C. Tip-In During Cornering

The tip-in during cornering maneuver consists of a step applied to the accelerator pedal while the vehicle is negotiating a turn. This test is used to investigate the variation in yaw rate and lateral acceleration after a step in the torque demand. As previously explained, one of the main tasks of this control system is to reduce the steady-state and dynamic variations in the understeer characteristic with a_x as much as possible.

Fig. 12 provides a comparison between suboptimal SOSM, PID, and the baseline vehicle in terms of a_y, r, and β, evaluated for an initial speed of $V = 90$ km/h with a step in torque demand, causing a sudden increase in the longitudinal acceleration of the vehicle of nearly 3 m/s^2. This provokes a significant perturbation in the yaw rate, lateral acceleration, and sideslip response of the baseline vehicle between 4 and 5 s. The phenomenon significantly affects the vehicle safety and comfort aspects. In real driving conditions, the driver would need to apply corrective actions via the steering wheel. The suboptimal SOSM allows the full compensation of the transient, with a performance benefit over the PID controller.

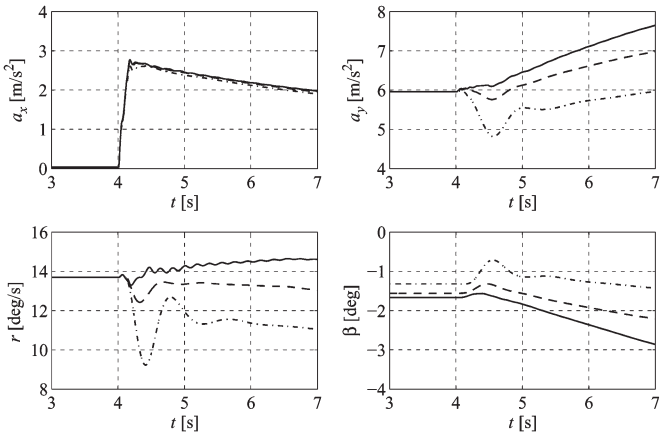

Fig. 12. Time histories of a_x, a_y, r, and β evaluated during the tip-in test at $V = 90$ km/h for (dotted-dashed line) the baseline vehicle, (dashed line) the vehicle with the PID controller, and (solid line) the vehicle with the suboptimal SOSM controller. Tire A has been used.

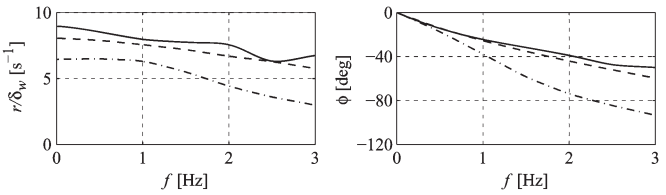

Fig. 13. Frequency response evaluated with sinusoidal steering inputs at different frequencies and amplitude of 10 deg for (dotted-dashed line) the baseline vehicle, (dashed line) the vehicle with the PID controller, and (solid line) the vehicle with suboptimal SOSM. Tire A has been used.

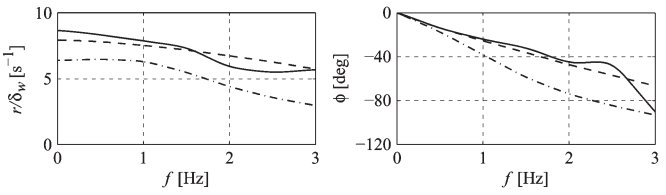

Fig. 14. Frequency response evaluated with sinusoidal steering inputs at different frequencies and amplitude of 20 deg for (dotted-dashed line) the baseline vehicle, (dashed line) the vehicle with the PID controller, and (solid line) the vehicle with suboptimal SOSM. Tire A has been used.

D. Frequency Response Analysis

The yaw rate frequency response characteristics have been evaluated with sinusoidal steering inputs of amplitudes 10 and 20 deg (Figs. 13 and 14, respectively) at $V = 90$ km/h and varying frequency for the PID, suboptimal SOSM, and the baseline vehicle, through simulations with the CarMaker-Simulink vehicle model.

The calculations show that the frequency response of the controlled vehicle with suboptimal SOSM varies to a large extent according to the amplitude of the steering inputs due to the high nonlinearity of the system. However, the suboptimal SOSM guarantees a marginally faster response (smaller magnitude of the phase angle) than the PID controller at least up to 2.7 Hz (see Fig. 14). On the other hand, for the PID algorithm, the variation in the yaw rate gain as a function of the input frequency is significantly smoother, showing monotonically decreasing behavior. Both controllers largely improve the magnitude and the phase angle response for the whole range of input frequencies.

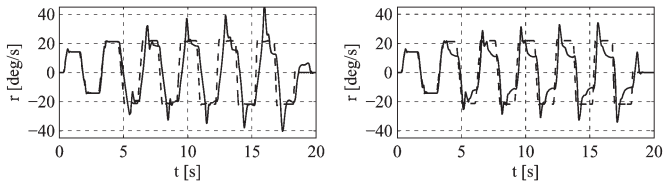

Fig. 15. Yaw rate r evaluated at $V = 90$ km/h and $\mu = 0.5$ during the sequence of step steer tests with (left) the suboptimal SOSM yaw rate controller and (right) the integrated yaw rate-sideslip angle controller. (Solid line) Actual yaw rate. (Dashed line) Trend of the reference yaw rate. Tire A has been used.

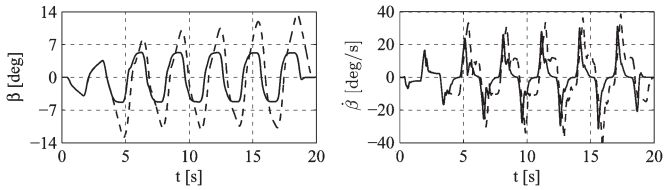

Fig. 16. Sideslip angle β and sideslip rate $\dot{\beta}$ evaluated at $V = 90$ km/h and $\mu = 0.5$ during the sequence of step steer tests with (dashed lines) the suboptimal SOSM yaw rate controller and (solid lines) the integrated yaw rate-sideslip angle controller. Tire A has been used.

VI. Assessment of the Integrated Yaw Rate and Sideslip Controller

To test the integrated yaw rate and sideslip angle controller, a sequence of step steer maneuvers with increasing amplitude has been simulated. If the friction estimation algorithm correctly works (condition omitted for brevity in the graphs of this section), the values of the yaw-rate-based PWF parameter are the same for the SOSM yaw rate controller and the integrated yaw rate and sideslip controller. In fact, the sideslip controller works as an additional safety feature of the yaw rate controller. This arrangement of the sideslip controller operating only in extreme conditions is particularly effective, as it does not require a precise estimation of sideslip angle and sideslip rate during normal driving, which is difficult even with the best state estimators available at the moment. Conversely, the existing state estimator technology is capable of detecting significant peaks of sideslip angle and sideslip rate, typical of extreme cornering maneuvers. As a consequence, for assessing the performance of the proposed integrated controller, a tire–road friction coefficient of $\mu = 0.5$ is considered, and a fault in the friction estimation is simulated so that the reference yaw rate is generated for $\mu = 1$ (otherwise, the sideslip controller would not be useful).

Fig. 15 shows the beneficial effect in terms of the yaw rate limitation when the sideslip angle controller is activated. Fig. 16 highlights that the sideslip angle is maintained within the specified threshold limits when the sideslip angle controller is active (solid line). The vehicle with the SOSM yaw rate controller only is characterized by peaks of sideslip angle in excess of 10 deg, which are beyond the limits that can be managed by nonprofessional drivers. Simulations at $\mu = 0.3$ have shown similar results and are omitted here for brevity.

VII. Conclusion

In this paper, a comparison of different yaw moment controllers has been presented, focusing on PID-based and sliding-mode algorithms. These are evaluated in the time and frequency domains. Furthermore, the effectiveness of an integrated sideslip controller within the overall control structure applied to maintain stability in emergency conditions has been investigated.

The results highlight the ability of the controllers to significantly change the understeer characteristic compared with the baseline vehicle. In the case of the PID controllers, a preliminary analysis in the frequency domain has shown that gain scheduling is not necessary for compensating variations in the vehicle yaw rate response at different operating points. Furthermore, in both quasi-steady-state maneuvers and typical transient tests, the PID algorithms allow good tracking performance and acceptable robustness against variations in the main vehicle parameters and operating conditions. The tracking performance in quasi-steady-state conditions is further enhanced by the suboptimal sliding-mode approach, which also achieves the objective of minimizing the variation in the vehicle yaw rate in acceleration conditions during tip-in maneuvers while cornering. However, the sliding-mode controllers can provoke undesirable oscillations in yaw rate during step steer maneuvers at high steering amplitudes. Overall, ease of implementation, predictable behavior, and good frequency response are key characteristics in favor of the PID controllers for real vehicle applications.

The integration of yaw rate and sideslip angle controllers creates a nested structure in which the yaw rate controller continuously works to achieve the reference cornering behavior, and the sideslip angle controller is used in case of inaccurate friction coefficient estimation or emergency conditions. Simulations have demonstrated the effectiveness of the proposed control structure.

References

[1] M. J. Hancock, R. A. Williams, E. Fina, and M. C. Best, "Yaw motion control via active differentials," *Trans. Inst. Meas. Control*, vol. 29, no. 2, pp. 137–158, Jun. 2007.

[2] A. van Zanten, R. Erhardt, and G. Pfaff, "VDC, The vehicle dynamics control system of Bosch," presented at the International Congress Exposition, Detroit, MI, USA, 1995, SAE Tech. Paper 950 749.

[3] G. Kaiser, Q. Liu, C. Hoffmann, M. Korte, and H. Werner, "Torque vectoring for an electric vehicle using an LPV drive controller and a torque and slip limiter," in *Proc. 51st IEEE Conf. Decision Control*, 2012, pp. 5016–5021.

[4] C. Poussot-Vassal, O. Sename, L. Dugard, and M. Savaresi, "Vehicle dynamic stability improvements through gain-scheduled steering and braking control," *Veh. Syst. Dyn.*, vol. 49, no. 10, pp. 1597–1621, Oct. 2011.

[5] S. Anwar, "Yaw stability control of an automotive vehicle via generalized predictive algorithm," in *Proc. Amer. Control Conf.*, 2005, pp. 435–440.

[6] Y. Shibahata, K. Shimada, and T. Tomari, "Improvement of vehicle maneuverability by direct yaw moment control," *Veh. Syst. Dyn.*, vol. 22, no. 5/6, pp. 465–481, Jan. 1993.

[7] M. Abe, "A theoretical analysis on vehicle cornering behaviors in acceleration and in braking," *Veh. Syst. Dyn.*, vol. 15, no. S1, pp. 1–14, Jan. 1986.

[8] M. Canale, L. Fagiano, A. Ferrara, and C. Vecchio, "Vehicle yaw control via second-order sliding-mode technique," *IEEE Trans. Ind. Electron.*, vol. 33, no. 11, pp. 3908–3916, Nov. 2005.

[9] B. Kwak and Y. Park, "Robust vehicle stability controller based on multiple sliding mode control," presented at the SAE World Congress, Detroit, MI, USA, 2001, Paper 2001-01-1060.

[10] H. B. Pacejka, *Tyre and Vehicle Dynamics,* 2nd ed. Oxford, U.K.: Butterworth-Heinemann, 2006.

[11] L. De Novellis, A. Sorniotti, P. Gruber, V. Ivanov, and K. Hoepping, "Torque vectoring control for electric vehicles with individually controlled motors: State-of-the-art and future developments," presented at the Electric Vehicle Symposium, Los Angeles, CA, USA, 2012, Paper 26.

[12] E-VECTOORC FP7 project. [Online]. Available: http:www.e-vectoorc.eu

[13] K. Sawase, Y. Ushiroda, and T. Miura, "Left–right torque vectoring technology as the core of Super All Wheel Control (S-AWC)," *Mitsubishi Motors Tech. Rev.*, vol. 18, pp. 18–24, Apr. 2006.

[14] L. De Novellis, A. Sorniotti, and P. Gruber, "Optimal wheel torque distribution for a four-wheel-drive fully electric vehicle," *SAE Int. J. Passenger Cars*, vol. 6, no. 1, pp. 128–136, May 2013.

[15] G. Genta, *Motor Vehicle Dynamics: Modelling and Simulation*. Singapore: World Scientific, 1997.

[16] W. F. Milliken and D. L. Milliken, *Chassis Design—Principles and Analysis*. Warrendale, PA, USA: SAE, 2002.

[17] L. De Novellis, A. Sorniotti, and P. Gruber, "Design and comparison of the handling performance of different electric vehicle layouts," *Proc. Inst. Mech. Eng. D, Autom. Eng.*, vol. 228, no. 2, pp. 218–232, Feb. 2014.

[18] T. Chung and K. Yi, "Design and evaluation of side slip angle-based vehicle stability control scheme on a virtual test track," *IEEE Trans. Control Syst. Technol.*, vol. 14, no. 2, pp. 224–234, Mar. 2006.

[19] F. Bottiglione, A. Sorniotti, and L. Shead, "The effect of half-shaft torsion dynamics on the performance of a traction control system for electric vehicles," *Proc. Inst. Mech. Eng. D, Autom. Eng.*, vol. 226, no. 9, pp. 1145–1159, Sep. 2012.

[20] W. F. Milliken and D. L. Milliken, *Race Car Vehicle Dynamics*. Warrendale, PA, USA: SAE, 1995.

[21] O. Mokhiamar and M. Abe, "Active wheel steering and yaw moment control combination to maximize stability as well as vehicle responsiveness during quick lane change for active vehicle handling safety," *Proc. Inst. Mech. Eng. D, Autom. Eng.*, vol. 216, no. 2, pp. 115–124, Feb. 2002.

[22] K. El Rifai, "Nonlinearly parameterized adaptive PID control for parallel and series realization," in *Proc. Amer. Control Conf.*, 2009, pp. 5150–5155.

[23] G. Bartolini, "Applications of a sub-optimal discontinuous control algorithm for uncertain second order systems," *Int. J. Robust Nonlin. Control*, vol. 7, no. 4, pp. 299–313, Apr. 1997.

[24] G. Bartolini, A. Ferrara, and E. Usai, "Chattering avoidance by second-order sliding mode control," *IEEE Trans. Autom. Control*, vol. 43, no. 2, pp. 241–246, Feb. 1998.

[25] G. Bartolini, A. Ferrara, A. Pisano, and E. Usai, "On the convergence properties of a 2-sliding control algorithm for non-linear uncertain systems," *Int. J. Control*, vol. 74, no. 7, pp. 718–731, Jan. 2001.

[26] A. Levant, "Sliding order and sliding accuracy in sliding mode control," *Int. J. Control*, vol. 58, no. 6, pp. 1247–1263, Dec. 1993.

[27] L. V. Levantovsky, "Second order sliding algorithms: Their realization," in *Proc. Dyn. Heterogeneous Syst. Conf.*, Moscow, Russia, 1985, pp. 32–43.

[28] C. A. Smith and A. Corripio, *Principles and Practice of Automatic Process Control*. Hoboken, NJ, USA: Wiley, 1997.

[29] C. Vecchio, "Sliding mode control: Theoretical developments and applications to uncertain mechanical systems," Ph.D. dissertation, Dept. Comput. Eng. Syst. Sci., Univ. Pavia, Pavia, Italy, 2008.

[30] M. Canale, L. Fagiano, A. Ferrara, and C. Vecchio, "Comparing internal model control and sliding-mode," *IEEE Trans. Intell. Transp. Syst.*, vol. 10, no. 1, pp. 31–41, Mar. 2009.

[31] J. J. E. Slotine and W. Li, *Applied Nonlinear Control*. Englewood Cliffs, NJ, USA: Prentice-Hall, 1991.

[32] A. Ferrara and M. Rubagotti, "A sub-optimal second order sliding mode controller with saturating actuators," in *Proc. Amer. Control Conf.*, Seattle, WA, USA, 2008, pp. 1082–1087.

[33] Z. L. Gaing, "A particle swarm optimization approach for optimum design of PID controller in AVR system," *IEEE Trans. Energy Convers.*, vol. 19, no. 2, pp. 384–391, Jun. 2004.

[34] *Passenger Cars—Steady-State Circular Driving Behaviour—Open-Loop Test Methods*, ISO Std. 4138:2012, 2012.

[35] M. Bauer, C. Ackermann, and R. Isermann, "Integrated state estimation with driving dynamic sensors and GPS data to evaluate driving dynamics control functions," presented at the FISITA World Automotive Congress, Beijing, China, 2012, Vol. 8, Paper F2012-E15-013, Vol. 8.

[36] E. Ono, T. Abe, and Y. Muragishi, "Vehicle stabilizing control apparatus," U.S.A, U.S. Patent 2006/0041 367 A1, Feb. 23, 2006.

Leonardo De Novellis (M'12) received the M.Sc. degree in mechanical engineering and the Ph.D. degree in mechanical and biomechanical design from Politecnico di Bari, Bari, Italy, in 2006 and 2010, respectively.

Since 2011, he has been a Research Fellow with the University of Surrey, Surrey, U.K. His main research interests include continuously variable transmissions and vehicle dynamics.

Aldo Sorniotti (M'12) received the M.Sc. degree in mechanical engineering and the Ph.D. degree in applied mechanics from Politecnico di Torino, Torino, Italy, in 2001 and 2005, respectively.

He is a Senior Lecturer in advanced vehicle engineering with the University of Surrey, Surrey, U.K. He is the E-VECTOORC (*E*lectric *Ve*hicle *C*ontrol of Individual Wheel *T*orque for *O*n- and *O*ff-*R*oad *C*onditions) project coordinator. His main research interests include vehicle dynamics control and transmissions for electric vehicles.

Patrick Gruber received the M.Sc. degree in motorsport engineering and management from Cranfield University, Cranfield, U.K., in 2005 and the Ph.D. degree in mechanical engineering from the University of Surrey, Surrey, U.K., in 2009.

Since 2009, he has been a Lecturer in advanced vehicle systems engineering with the University of Surrey. His current research is in the field of tire dynamics and the development of novel tire models.

Andrew Pennycott received the M.Eng. and the Ph.D. degrees in mechanical engineering from the University of Glasgow, Glasgow, U.K., in 2004 and 2008, respectively.

Since 2012, he has been a Research Fellow with the University of Surrey, Surrey, U.K. His research is focused on control engineering for automotive and rehabilitation applications.